



# Identification of a 1.4-kb-Long Sequence Located in the nsp12 and nsp13 Coding Regions of SARS-CoV-2 Genomic RNA That Mediates Efficient Viral RNA Packaging

✉ Kaori Terasaki,<sup>a,b</sup> Krishna Narayanan,<sup>a</sup> ✉ Shinji Makino<sup>a,b,c,d,e</sup>

<sup>a</sup>Department of Microbiology and Immunology, The University of Texas Medical Branch, Galveston, Texas, USA

<sup>b</sup>Institute for Human Infections and Immunity, The University of Texas Medical Branch, Galveston, Texas, USA

<sup>c</sup>Center for Biodefense and Emerging Infectious Diseases, The University of Texas Medical Branch, Galveston, Texas, USA

<sup>d</sup>UTMB Center for Tropical Diseases, The University of Texas Medical Branch, Galveston, Texas, USA

<sup>e</sup>The Sealy Institute for Vaccine Sciences, The University of Texas Medical Branch, Galveston, Texas, USA

**ABSTRACT** The specific packaging of the viral RNA genome into virus particles is an essential step in the replication cycle of coronaviruses (CoVs). Using a single-cycle, replicable severe acute respiratory syndrome CoV-2 (SARS-CoV-2) mutant, we demonstrated the preferential packaging of the SARS-CoV-2 genomic RNA into purified virus particles. Furthermore, based on the sequence of an efficiently packaged defective interfering RNA of SARS-CoV, a closely related CoV, that was generated after serial passages of SARS-CoV in cell culture, we designed a series of replication-competent SARS-CoV-2 minigenome RNAs to identify the specific viral RNA region that is important for SARS-CoV-2 RNA packaging into virus particles. We showed that a 1.4-kb-long sequence, derived from the nsp12 and nsp13 coding regions of the SARS-CoV-2 genomic RNA, is required for the efficient packaging of SARS-CoV-2 minigenome RNA into SARS-CoV-2 particles. In addition, we also showed that the presence of possibly the entire 1.4-kb-long sequence is important for the efficient packaging of SARS-CoV-2 RNA. Our findings highlight the differences between the RNA packaging sequence identified in SARS-CoV-2, a Sarbecovirus, and the packaging signal of mouse hepatitis virus (MHV), an Embecovirus, which is a 95-nt-long sequence located at the nsp15 coding region of MHV genomic RNA. Collectively, our data imply that both the location and the sequence/structural features of the RNA element(s) that drives the selective and efficient packaging of viral genomic RNA are not conserved among the subgenera Embecovirus and Sarbecovirus within the Betacoronavirus genus.

**IMPORTANCE** Elucidating the mechanism of SARS-CoV-2 RNA packaging into virus particles is important for the rational design of antiviral drugs that inhibit this vital step in the replication cycle of CoVs. However, our knowledge about the RNA packaging mechanism in SARS-CoV-2, including the identification of the viral RNA region important for SARS-CoV-2 RNA packaging, is limited, primarily due to the logistical challenges of handling SARS-CoV-2 in biosafety level 3 (BSL3) facilities. Our study, using a single-cycle, replicable SARS-CoV-2 mutant, which can be handled in a BSL2 lab, demonstrated the preferential packaging of full-length SARS-CoV-2 genomic RNA into virus particles and identified a specific 1.4-kb-long RNA region in SARS-CoV-2 genomic RNA that is required for the efficient packaging of SARS-CoV-2 RNA into virus particles. The information generated in our study could be valuable for clarifying the mechanisms of SARS-CoV-2 RNA packaging and for the development of targeted therapeutics against SARS-CoV-2 and other related CoVs.

**KEYWORDS** coronavirus, packaging signal, SARS-CoV-2, viral genome packaging

**Editor** Tom Gallagher, Loyola University Chicago-Health Sciences Campus

**Copyright** © 2023 American Society for Microbiology. All Rights Reserved.

Address correspondence to Kaori Terasaki, katerasa@utmb.edu, or Shinji Makino, shmakino@utmb.edu.

The authors declare no conflict of interest.

**Received** 10 May 2023

**Accepted** 9 June 2023

The coronavirus disease (COVID-19) pandemic caused by SARS-CoV-2, a novel human coronavirus, has had serious negative impacts on public health and global economy with over 6 million deaths worldwide. SARS-CoV-2 infection primarily causes cold-like symptoms, including fever, cough, and headache, but some patients develop more severe respiratory diseases due to lung tissue damage (1). Accumulating evidence has shown that the systemic manifestations of SARS-CoV-2 infection extends beyond acute respiratory disease (2, 3). Currently, the circulating Omicron variants of SARS-CoV-2 are highly transmissible, causing an adverse effect on human health due to immune evasion in the vaccinated population (4). Several commercial vaccines designed to express the spike protein of the WA1/2020 strain and the Omicron strain are available and effective at preventing severe COVID-19 (5). However, there is only one antiviral drug approved by the Food and Drug Administration (FDA) to treat SARS-CoV-2 patients (6).

SARS-CoV-2, which belongs to the family *Coronaviridae* and order *Nidovirales*, is an enveloped virus carrying a single-stranded positive-sense RNA genome. Among the six different CoV genera (Alphacoronavirus, Betacoronavirus, Gammacoronavirus, Deltacoronavirus, Alphapirnavirus, and Alphaletovirus) in the family *Coronaviridae*, SARS-CoV-2 and SARS-CoV belong to the genus *Betacoronavirus*, subgenus *Sarbecovirus*. The CoV virion is generally composed of three envelope proteins, namely, S, M, and E, and a helical nucleocapsid composed of N protein and a large (~30 kb) single-stranded positive-sense RNA genome, carrying a 5' cap and a poly(A) tail at the 3'-end (7). The S protein plays a critical role in the binding of CoV particles to a specific receptor and induces membrane fusion (8). The E protein is essential for virion assembly and budding for some, but not all, CoVs (9). The M protein, which represents the most abundant viral protein, interacts with other envelope proteins and the N protein as well as the viral RNA and plays a central role in virion assembly (10, 11). In infected cells, the intracellular form of the viral genomic RNA, mRNA1, and several subgenomic mRNAs are synthesized. These viral mRNAs form a 3' coterminal nested structure and have the same leader sequence of ~70 nt at the 5' end (7). All viral mRNAs, except for the smallest subgenomic mRNA, are structurally polycistronic, and the most 5' open reading frame (ORF) is, in principle, used for translation (7). The 5' two-thirds of the genomic RNA is called gene 1, which encodes 16 mature nonstructural proteins (nsp1 to nsp16) in the case of betaCoVs. Most of the gene 1 proteins are essential for viral RNA synthesis (12).

CoV particles primarily contain the genomic RNA and very small amounts of subgenomic mRNAs (13–15). The packaging of genomic RNA into virus particles is a critical step in the infectious cycle of CoVs. The selective packaging of genomic RNA into CoV particles is driven by an RNA element designated the packaging signal (PS). Among the CoV PSs, the PS of mouse hepatitis virus (MHV), a member of the *Embecovirus* subgenus in the betaCoV genus, has been well characterized. MHV carries a 95-nucleotide (nt)-long PS within the nsp15 coding region of gene 1 (16). MHV M interacts with MHV mRNA 1 and replicating MHV defective interfering (DI) RNAs carrying PS but not subgenomic mRNAs and DI RNAs lacking PS (17), indicating that the binding of M protein to PS is a determinant of the packaging efficiency of viral RNAs. The importance of N protein for the selective packaging of genomic RNA has also been reported (17–19). The existing experimental evidence suggest that the genomic RNA, carrying the PS, can outcompete the subgenomic RNAs, which lack the PS, for interactions with the structural proteins, namely, M and N, that drive the process of selective genomic RNA packaging into virus particles (15).

The identification of viral RNA PS and clarifying the mechanism of viral RNA packaging in highly pathogenic human CoVs, including SARS-CoV, SARS-CoV-2, and Middle East respiratory syndrome (MERS)-CoV, has been challenging, due to the technical hurdles of performing the necessary experiments, including the purification of infectious CoVs in biosafety level 3 (BSL3) labs. Based on the data from other CoVs that can be handled in BSL2 labs, it has been speculated that the full-length genomic RNA of these highly pathogenic human CoVs is also selectively packaged into virus particles. However, the experimental data demonstrating the selective packaging of genomic RNA, but not subgenomic mRNAs, into virus particles of these CoVs is still lacking. Several studies have shown the packaging of expressed RNA carrying a putative PS into SARS-CoV virus-like particles (VLPs) (20), SARS-CoV-2 VLPs

(21), or MERS-CoV VLPs (22). These studies have suggested the presence of a putative PS in the genomic RNA of SARS-CoV and SARS-CoV-2 in the same region identified as the PS in MHV genomic RNA, i.e., the nsp15 region of gene 1 (20, 21). However, the sequence corresponding to MHV PS is absent in Sarbecoviruses, and the putative PS of SARS-CoV and that of SARS-CoV-2 lack the conserved RNA structural features found in the PS of other CoVs (23), suggesting that the PS of SARS-CoV and SARS-CoV-2 are located elsewhere in the genome.

The present study aimed to identify the specific region in SARS-CoV-2 RNA that is important for the efficient packaging of viral RNA into SARS-CoV-2 particles, by primarily using a single-cycle, replicable SARS-CoV-2 mutant (srSARS-CoV-2), which is a BSL2 pathogen (24). We showed that the genomic RNAs, but not subgenomic mRNAs, are efficiently packaged into purified srSARS-CoV-2 particles. Furthermore, using a series of replication-competent SARS-CoV-2 minigenome RNAs, we showed the requirement of a ~1.4-kb-long sequence, derived from the nsp12 and nsp13 coding regions of the genomic RNA, for the efficient packaging of SARS-CoV-2 minigenome RNA into SARS-CoV-2 particles, which suggested that the structure/sequence of the RNA element(s) that drives the selective and efficient packaging of SARS-CoV-2 RNA is different from that in MHV.

## RESULTS

**Efficient packaging of genomic RNA, but not subgenomic mRNAs, into SARS-CoV-2 virions.** As a first step toward the goal of identifying the specific region in SARS-CoV-2 RNA that mediates the packaging of viral RNA into SARS-CoV-2 particles, we examined the packaging profile of viral RNAs in SARS-CoV-2 particles by using a single-cycle, replicable SARS-CoV-2 mutant (srSARS-CoV-2), which was initially referred to as SARS2-delORF3-E virus (24), as a surrogate for SARS-CoV-2. srSARS-CoV-2 lacks E and 3a genes, carries a NanoLuc luciferase gene (24), and undergoes a full cycle of virus replication, including the production of virus particles, capable of initiating infection in Vero-ORF3-E cells, coexpressing SARS-CoV-2 3a and E proteins (24). However, srSARS-CoV-2 exhibits a single-cycle, replication property in cells lacking the coexpression of E and 3a proteins (24).

To test whether the genomic RNA of srSARS-CoV-2 is preferentially packaged into virions, we first examined the profile of accumulation of viral RNAs in cells infected with srSARS-CoV-2 and compared it to that in cells infected with infectious SARS-CoV-2. Northern blot analysis showed the accumulation of mRNA 1, the intracellular form of the genomic RNA, and subgenomic mRNAs in Vero E6 cells infected with SARS-CoV-2, as well as in srSARS-CoV-2-infected Vero-ORF3-E cells, coexpressing 3a and E proteins (Fig. 1C, IC). Due to the deletion of E and ORF3 genes in srSARS-CoV-2, the accumulation of mRNA 3, encoding 3a, and mRNA 4, encoding E, did not occur in srSARS-CoV-2-infected cells. As the mRNA 7 of srSARS-CoV-2 carries a 516-nt-long NanoLuc luciferase gene in place of the 366-nt-long ORF7 gene (24), the sizes of mRNAs 5, 6, and 7 of srSARS-CoV-2 were larger than the corresponding mRNAs of SARS-CoV-2. We also detected some noncanonical subgenomic RNAs in srSARS-CoV-2-infected cells, which most probably represented aberrant transcripts (Fig. 1C, asterisk). We inoculated srSARS-CoV-2 into Vero-ORF3-E cells, coexpressing E and 3a proteins, and purified the released virus particles by using continuous sucrose gradient centrifugation. Western blot analysis of the sucrose gradient fractions showed an enrichment of the viral M protein in fractions 6 and 7, with buoyant densities between 1.164 and 1.187 g/mL, suggesting the presence of purified virus particles in these fractions (Fig. 1A and B). Northern blot analysis of the RNAs extracted from the sucrose gradient fractions, by using a 3'-end probe which binds to both the genomic and subgenomic mRNAs of SARS-CoV-2, showed the presence of genomic RNA in fractions 6 to 8 with the strongest signal in fraction 7 (Fig. 1C, virion). Very low amounts of subgenomic mRNAs were detected in fractions 6 and 7, and the ratio of genomic RNA to subgenomic mRNAs in the purified virion was higher than that in infected cells. These data demonstrated that the full-length genomic RNA is preferentially packaged into srSARS-CoV-2 particles, released from infected cells.

**Characterization of a SARS-CoV defective interfering (DI) RNA.** DI RNAs have been used to identify the *cis*-acting sequences required for CoV RNA replication and packaging in other CoVs (16). To this end, we had previously performed serial, undiluted passages of SARS-CoV in Vero E6 cells during the SARS-CoV outbreak in 2002 to 2003 to generate DI

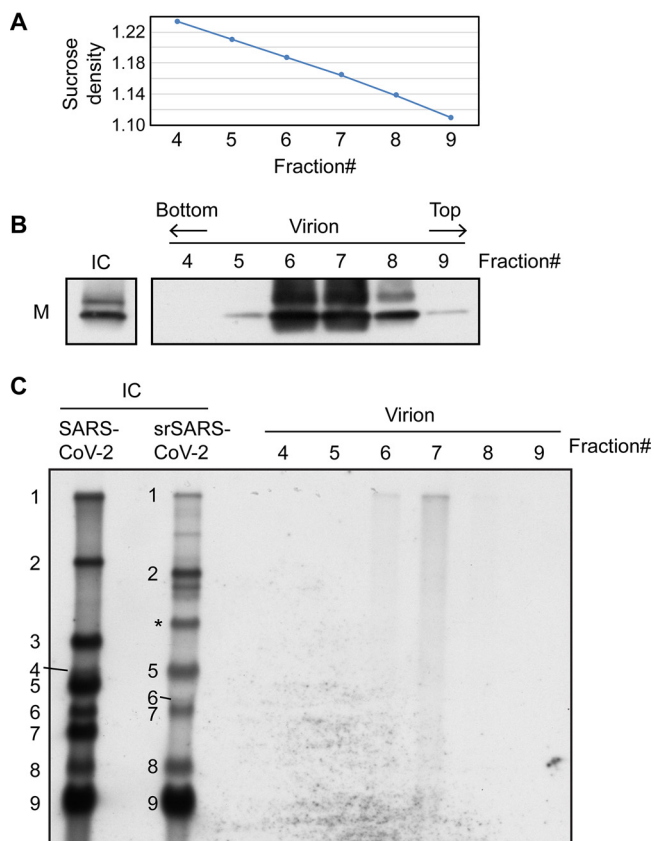


**FIG 1** Preferential packaging of srSARS-CoV-2 genomic RNA into purified virions. (A) The virus particles released from srSARS-CoV-2-infected cells were subjected to continuous sucrose gradient ultracentrifugation, and the gradient fractions were collected. The density of each sucrose fraction was measured using a refractometer. The density of sucrose fractions 4 to 9 are shown. (B) Western blot analysis of M protein in srSARS-CoV-2-infected Vero-ORF3-E cells (IC) and in sucrose gradient fractions 4 to 9. (C) Northern blot analysis of total intracellular RNAs (IC), in SARS-CoV-2-infected cells and srSARS-CoV-2-infected cells, and virion RNAs in sucrose gradient fractions 4 to 9 (Virion). The intracellular viral mRNA species of SARS-CoV-2 and srSARS-CoV-2 are indicated by the numbers 1 to 9. The asterisk indicates the noncanonical subgenomic RNA in srSARS-CoV-2-infected cells.

RNAs in SARS-CoV-infected cells. We first examined the accumulation of intracellular viral RNAs in cells infected with the passaged virus samples (Fig. 2A). Northern blot analysis of intracellular RNAs in infected cells, by using a 5'-end probe, which hybridizes to the genomic RNA/mRNA 1, but not subgenomic mRNAs of SARS-CoV, showed the accumulation of mRNA 1 and a major viral RNA species of ~5.5 kb in length in cells infected with virus inoculum from passages 14 to 23. Northern blot analysis using a 3'-end probe, which binds to all SARS-CoV mRNA species, also showed the accumulation of the 5.5-kb-long RNA species (Fig. 2A). Importantly, the accumulation of SARS-CoV mRNA 1 and subgenomic mRNAs was markedly reduced in cells infected with the serially passaged virus, with the most prominent reduction observed in cells infected with passage 17 to passage 23 inoculum (Fig. 2A). These data suggested that the 5.5-kb-long RNA species was stably retained in the serially passaged virus and its accumulation interfered with SARS-CoV replication, strongly indicating that the 5.5-kb-long RNA species was a SARS-CoV DI RNA that is efficiently packaged into SARS-CoV particles. Sequence analysis showed that the SARS-CoV DI RNA is composed of three distinct and noncontiguous regions of the SARS-CoV genome, as follows: the first 740-nt-long sequence from the 5' end of the genome, an internal sequence derived from the nsp7 to nsp13 coding region encompassing nt 11976 to 16382, and the terminal 600-nt-long region from the 3' end of the SARS-CoV genome (Fig. 2B). Like other CoV DI RNAs (13, 25–27), this DI RNA also encoded an open reading frame (ORF), carrying the first 475 nt of nsp1 in frame with the internal sequence encompassing nt 11976 to 16382 (Fig. 2B). The terminal 600-nt-long region from the 3' end of the genome also carried a partial ORF derived

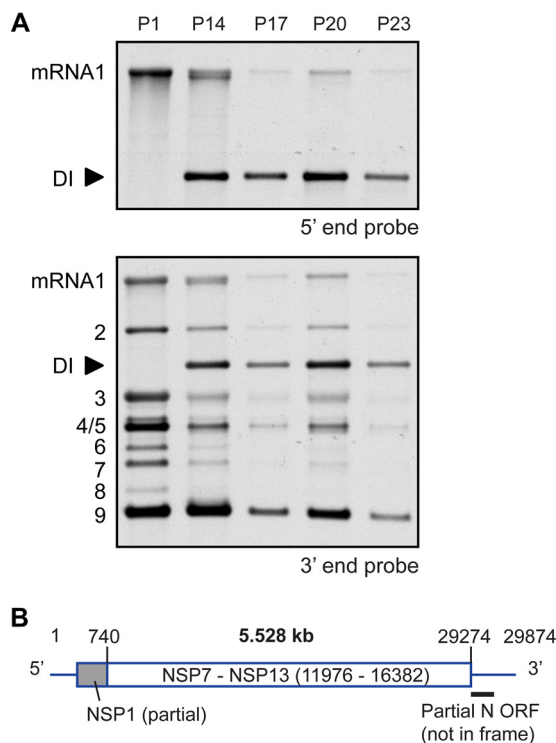


**FIG 2** Characterization of SARS-CoV DI RNA after serial passage of SARS-CoV in Vero E6 cells. (A) Northern blot analysis of total RNAs extracted from Vero E6 cells infected with serially passaged SARS-CoV using the 5'-end probe (top) and the 3'-end probe (bottom). The passage numbers of the serially passaged SARS-CoV are indicated. (B) Schematic diagram of the structure of SARS-CoV DI RNA.

from the N gene, but this ORF was not in frame with the upstream ORF. Notably, the SARS-CoV DI RNA lacked the previously suggested putative PS sequence of SARS-CoV that mapped to the nsp15 region (20). The SARS-CoV DI RNA also did not carry the sequence corresponding to the putative SARS-CoV-2 PS that mapped within the nsp15 and nsp16 regions (21).

**Evaluating the packaging efficiency of SARS-CoV-2 minigenome RNAs.** As SARS-CoV-2 is closely related to SARS-CoV, we hypothesized that the RNA element(s) required for the efficient packaging of viral RNA would be located at a similar site in the genome of both CoVs. To identify the viral RNA region that drives the packaging of SARS-CoV-2 RNA into virus particles, we generated a series of replication-competent SARS-CoV-2 minigenome RNAs, designated SARS2-rep RNAs (Fig. 3A), based on the sequence of the SARS-CoV DI RNA. All the SARS2-rep RNAs carried the following common regions derived from the SARS-CoV-2 genome at their 5' and 3' ends: the first 742 nt from the 5' end and the terminal 605 nt from the 3' end of the SARS-CoV-2 genome, respectively (Fig. 3A). In addition, each of the SARS2-rep RNAs used in our study carried a different internal fragment (designated F1 to F7), ranging in length from 1 kb to 1.7 kb, derived from the nsp7 to the nsp16 coding regions of SARS-CoV-2 (Fig. 3B). As a previous study suggested the presence of the SARS-CoV-2 PS at the nsp15 and nsp16 coding regions (21), we included the SARS2-rep RNA covering the coding regions of nsp14 to nsp16 (designated F4 to F7) for our study, although this region was lacking in the SARS-CoV DI RNA. For a negative control, we generated the SARS2-rep-rLuc RNA, in which the *Renilla* luciferase (rLuc) gene was inserted as the internal sequence instead of the coding regions from SARS-CoV-2 genome (Fig. 3A). All the SARS2-rep RNAs carried an ORF, consisting of a partial N-terminal sequence of nsp1 in frame with the internal sequence encompassing the nsp7 to the nsp16 coding regions. The SARS2-rep-rLuc RNA encoded an ORF, consisting of the partial nsp1 sequence in-frame with the rLuc gene.

We first tested the replication competence of SARS2-rep RNA by transfecting each of the SARS2-rep RNAs or SARS2-rep-rLuc RNA into SARS-CoV-2-infected Vero E6 cells, wherein SARS-CoV-2 served as a helper virus. As a negative control, the RNAs were transfected into mock-infected cells. Northern blot analysis of intracellular RNAs from the transfected Vero E6

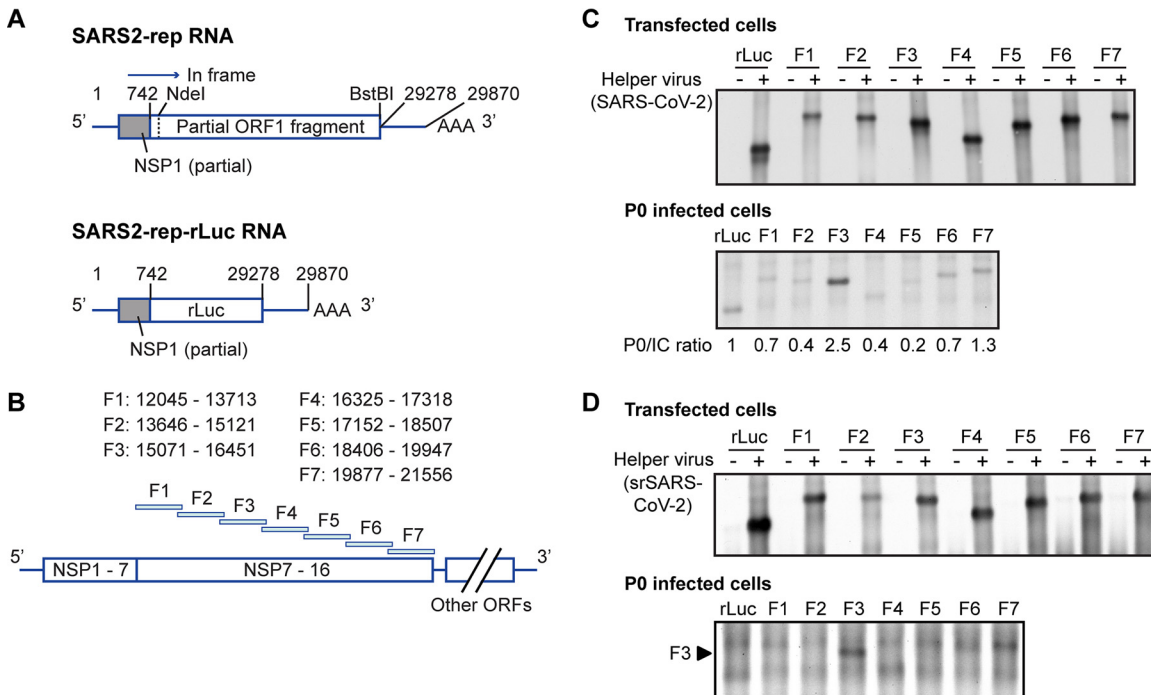


**FIG 3** Packaging efficiency of SARS2-rep RNAs. (A) Schematic diagram of SARS2-rep RNAs and SARS2-rep-rLuc RNA. (B) Schematic diagram of the SARS-CoV-2 genome. The location and the nucleotide positions of the F1 to F7 regions in the SARS-CoV-2 genome are indicated. (C) Accumulation of SARS2-rep RNAs in SARS-CoV-2-infected cells. Vero E6 cells were infected with SARS-CoV-2 (Helper virus +) or mock infected (Helper virus -) and then transfected with *in vitro*-synthesized SARS2-rep RNAs (F1 to F7) or SARS2-rep-rLuc RNA (rLuc). Culture supernatants (P0 virus) were collected and used for inoculating naive Vero E6 cells. Total RNAs were extracted from the transfected cells and P0-infected cells and analyzed by Northern blotting using the SARS-CoV-2 5'-end probe. The P0/IC ratio of the given SARS2-rep RNA species was calculated by dividing the band intensity of that RNA in P0-infected cells (P0) by that in transfected cells (IC). (D) Accumulation of SARS2-rep RNAs in srSARS-CoV-2-infected cells. Vero-ORF3-E cells were infected with srSARS-CoV-2 (Helper virus +) or mock infected (Helper virus -) followed by transfection with *in vitro*-synthesized SARS2-rep RNAs or SARS2-rep-rLuc RNA. Culture supernatants (P0 virus) were harvested and used for infecting fresh Vero-ORF3-E cells. Total RNAs were extracted from the transfected cells and P0-infected cells and analyzed by Northern blotting using the SARS-CoV-2 5'-end probe.

cells showed that the SARS2-rep RNAs as well as the SARS2-rep-rLuc RNA replicated efficiently in SARS-CoV-2-infected cells but not in mock-infected cells, confirming their replication competence (Fig. 3C).

To evaluate the efficiency of packaging SARS2-rep RNAs into SARS-CoV-2 particles, we collected the culture supernatants (P0 virus) from SARS-CoV-2-infected Vero E6 cells that were transfected with each of the SARS2-rep RNAs or SARS2-rep-rLuc RNA, at 19 h postinfection (p.i.) and inoculated naive Vero E6 cells with the P0 virus. Northern blot analysis of intracellular RNAs from P0-infected cells showed that the accumulation of SARS2-rep RNA carrying the F3 internal fragment (F3 RNA), derived from the nsp12 and nsp13 coding regions of SARS-CoV-2 genome, was higher than that of other SARS2-rep RNAs and SARS2-rep-rLuc RNA (Fig. 3C). The packaging efficiency (P0/IC) of the SARS2-rep RNAs was calculated as the ratio of the amount of intracellular RNA (IC) in RNA-transfected cells (replication competence) and in P0-infected cells (P0) (packaging competence) by quantifying the band intensity using densitometry. The P0/IC ratio of F3 RNA was higher than that of other SARS2-rep RNAs and SARS2-rep-rLuc RNA (Fig. 3C), suggesting that the F3 RNA, but not other minigenome RNAs, was efficiently packaged into SARS-CoV-2 particles released from the RNA-transfected cells, resulting in the efficient accumulation of F3 RNA in P0-infected cells.

We repeated these experiments using srSARS-CoV-2 as a helper virus to confirm our results. srSARS-CoV-2-infected Vero-ORF3-E cells, coexpressing E and 3a proteins, were transfected with each of the SARS2-rep RNAs or SARS2-rep-rLuc RNA. P0 virus samples were collected at 24 to 30 h p.i. and inoculated into naive Vero-ORF3-E cells. As observed in Fig. 3C using SARS-CoV-2 as the helper virus, Northern blot analysis of intracellular RNAs from P0-infected cells also showed a higher accumulation of F3 RNA than that of other minigenome RNAs (Fig. 3D). We did not calculate the P0/IC ratio for these samples

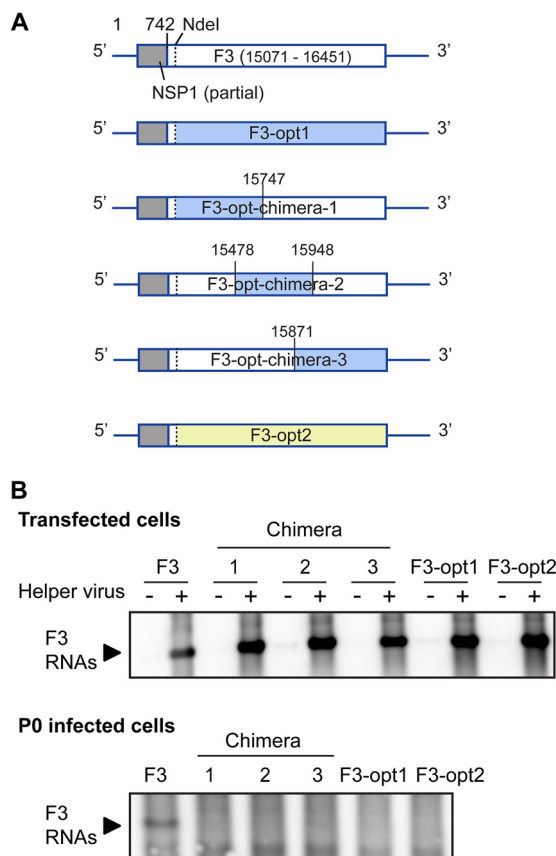


**FIG 4** Packaging efficiency of F3 RNA variants. (A) Schematic diagrams of F3 RNA variants, F3-opt1, F3-opt2, and F3-opt-chimeras. (B) Accumulation of F3 RNA variants in srSARS-CoV-2-infected cells. Experiments were performed as described in Fig. 3, except that F3 RNA variants were used for transfection into srSARS-CoV-2-infected Vero-ORF3-E cells.

due to the high background signals in P0-infected samples, which prevented the accurate quantification of the band intensities of P0 RNAs. Nevertheless, our data, using SARS-CoV-2 and srSARS-CoV-2 as helper viruses, strongly suggested that SARS2-rep RNA, carrying the F3 region, is efficiently packaged into virus particles.

To examine whether the RNA secondary structures in the F3 region are important for efficient F3 RNA packaging, we tested the effect of changing the primary nucleotide sequence of the F3 region for RNA packaging. We utilized the codon optimization strategy to alter the nucleotide sequence of F3 RNA, which does not change the amino acid sequence but probably alters the RNA secondary structures in the F3 RNA. We generated two different variants of F3 RNA (Fig. 4A), namely, F3-opt1, carrying *E. coli*-codon optimized F3 region, and F3-opt2, carrying a bovine codon-optimized F3 region. To further identify the specific region responsible for the efficient packaging of F3 RNA, we generated three additional chimeric variants, namely, F3-opt-chimera-1, F3-opt chimera-2, and F3-opt-chimera-3, with each carrying a chimeric F3 sequence derived from F3 and F3-opt1, as shown in Fig. 4A. All these variants had the same nucleotide length as F3 RNA. We examined the packaging abilities of these F3 RNA-derived variants, as described in Fig. 3D, by using srSARS-CoV-2 as a helper virus. Northern blot analysis of intracellular RNAs from transfected cells showed that all the F3 RNA-derived variants replicated efficiently in the presence of the helper virus, srSARS-CoV-2 (Fig. 4B). However, the accumulation of all the F3 RNA-derived variants in P0-infected cells was substantially lower than that of F3 RNA, suggesting that these variants were not efficiently packaged into srSARS-CoV-2 particles. Furthermore, our data also indicated the importance of potentially the entire 1.4-kb-long F3 sequence for the efficient packaging of SARS2-rep RNA into virus particles.

**Importance of the 1.4-kb-long F3 region for packaging minigenome RNA into virus particles.** To directly assay the efficient packaging of F3 RNA, but not F3-opt1 RNA, into virus particles, we purified the srSARS-CoV-2 particles, released from

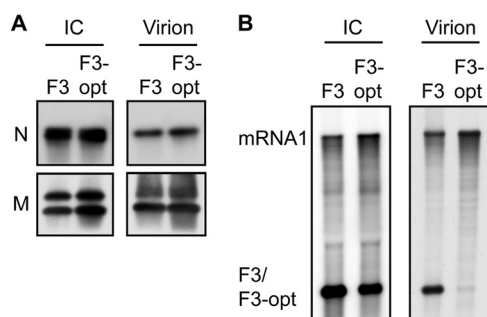


**FIG 5** Efficient packaging of F3 RNA, but not F3-opt1 RNA, into purified srSARS-CoV-2 particles. srSARS-CoV-2-infected Vero-ORF3-E cells were transfected with F3 RNA or F3-opt1 RNA. Culture supernatants were harvested at 27 h p.i., and the released virus particles in the culture supernatant were purified by sucrose gradient ultracentrifugation. (A) Western blot analysis of the intracellular lysate (IC) and purified virions (Virion) to detect SARS-CoV-2 N and M proteins. (B) Northern blot analysis of the total RNA extracted from the intracellular lysate (IC) and purified virions (Virion) using the SARS-CoV-2 5'-end probe.

srSARS-CoV-2-infected Vero-ORF3-E cells that were transfected with F3 RNA or F3-opt1 RNA. Western blot analysis of intracellular lysates (ICs) and purified virus particles (virion), using anti-M antibody and anti-N antibody showed similar levels of M and N proteins in both samples, indicating that similar amounts of virus particles were released from F3 RNA- and F3-opt1 RNA-transfected cells (Fig. 5A). Northern blot analysis of intracellular RNAs showed the efficient and comparable accumulation of both F3 RNA and F3-opt1 RNA in RNA-transfected cells, whereas the amount of genomic RNA (marked as mRNA 1) was slightly higher in the sample transfected with F3-opt1 RNA than that with F3 RNA (Fig. 5B). Importantly, the amount of F3 RNA in the purified virions was substantially higher than that of F3-opt1, despite the similar intracellular levels of accumulation of both RNAs (Fig. 5B). Our data directly demonstrated that F3 RNA, but not F3-opt1 RNA, is efficiently packaged into srSARS-CoV-2 particles, confirming our results obtained using the indirect packaging assay in Fig. 3 and 4.

## DISCUSSION

In the present study, we first experimentally demonstrated that the genomic RNA, but not the subgenomic RNAs of srSARS-CoV-2, which was used as a surrogate for SARS-CoV-2, is efficiently packaged into purified srSARS-CoV-2 particles (Fig. 1). The selective packaging of genomic RNA into srSARS-CoV-2 particles suggested the presence of a region(s) in the genomic RNA of srSARS-CoV-2 that promotes its efficient packaging into virus particles.

As DI RNAs have been used to identify the RNA PS in other CoVs, we first analyzed the sequence of a SARS-CoV DI RNA that was generated previously in our laboratory after serial passages of SARS-CoV in Vero E6 cells. The stable retention of the SARS-CoV DI RNA in the serially passaged virus strongly indicated that the DI RNA was efficiently packaged into SARS-CoV particles and, therefore, most probably carried an RNA PS. As SARS-CoV and SARS-CoV-2 are closely related CoVs, in order to identify the region that contributed to the efficient packaging of SARS-CoV-2 genome, we generated a series of replication-competent SARS2-rep RNAs, carrying noncontiguous regions of the SARS-CoV-2 genome, based on the sequence of the SARS-CoV DI RNA. Our indirect packaging assay using SARS2-rep RNAs, carrying different internal fragments (F1 to F7) derived from the nsp7 to nsp16 coding regions of the SARS-CoV-2 genome, suggested the efficient packaging of F3 RNA into srSARS-CoV-2 and SARS-CoV-2 particles (Fig. 3). We also directly demonstrated the efficient packaging of F3 RNA into purified srSARS-CoV-2 particles, confirming our results from the indirect packaging assay (Fig. 5). As the F3 RNA carried sequences from the nsp12 and nsp13 coding regions of the SARS-CoV genome, our data indicated that this region is also important for the efficient packaging of SARS-CoV-2 genomic RNA into virus particles. In addition, the inefficient packaging of the F3-opt-chimeras, which carried up to 800 nt of the F3 region-derived RNA sequence, suggested that the presence of possibly the entire 1.4-kb-long region or at least more than 800 nt of the F3 RNA region is required for the efficient packaging of viral RNA

into SARS-CoV-2 particles (Fig. 4B). Furthermore, our data showing that sequences in the nsp12 and nsp13 coding regions of the SARS-CoV-2 genome are important for viral RNA packaging highlight the different locations of the putative SARS-CoV-2 PS and MHV PS, which mapped to the nsp15 region of the MHV genome.

Others have reported the generation of SARS-CoV-2 DI RNAs (28), which accumulated efficiently during serial passages of SARS-CoV-2 and inhibited SARS-CoV-2 replication. Although the packaging efficiencies of these DI RNAs were not experimentally determined, the presence of these DI RNAs in the passaged virus samples suggested that these DI RNAs can be efficiently packaged into SARS-CoV-2 particles. Importantly, these DI RNAs also carried the F3 RNA sequence, along with other regions of the SARS-CoV-2 genome, further supporting our data that sequences in the nsp12 and 13 coding region of the SARS-CoV-2 genome are important for viral RNA packaging into SARS-CoV-2 particles.

Previously, a putative SARS-CoV-2 PS was identified by examining the packaging of a series of expressed SARS-CoV-2 RNA fragments, each of which carried a different region of gene 1, into SARS-CoV-2 VLPs (21). Among the expressed RNA fragments, RNA T20, carrying nt 20080 to 22222 (T20 region) of the SARS-CoV-2 genome, was most efficiently packaged into the VLPs (21), implying that the T20 region includes an RNA element(s) that facilitates viral RNA packaging into SARS-CoV-2 VLPs. However, the SARS-CoV-2 DI RNAs did not carry the sequences corresponding to the T20 region (28), suggesting that the T20 region may not be as efficient as the F3 region, identified in our study, for the packaging of SARS-CoV-2 genomic RNA. Furthermore, the packaging efficiencies of T15 and T16 RNAs, carrying nt 14010 to 16085 and nt 16011 to 18186 of the SARS-CoV-2 genome, respectively, were lower than that of the T20 RNA. As these RNAs carried only a part of the F3 sequence, it is possible that the inefficient packaging of these RNAs into SARS-CoV-2 VLPs could be due to the absence of the entire F3 sequence, further confirming our data in Fig. 4.

As SARS-CoV and SARS-CoV-2 are closely related CoVs, it is highly likely that the selective and efficient packaging of their genomic RNAs is mediated by a specific RNA region that is located at a similar site in their genomes. Our study using SARS-CoV DI RNA, which was stably retained during serial passage of SARS-CoV in Vero E6 cells and inhibited SARS-CoV mRNA synthesis (Fig. 2), strongly suggested that it was efficiently packaged into SARS-CoV particles. As the SARS-CoV DI RNA carried the region of SARS-CoV genome corresponding to the F3 region of SARS-CoV-2, it is reasonable to speculate that this specific RNA region in the SARS-CoV genome is also important for viral RNA packaging into SARS-CoV particles.

To identify the presence of conserved RNA structural elements among the F3 region of SARS-CoV-2 and the corresponding region of the SARS-CoV genome, we compared the RNA secondary structures of these regions in SARS-CoV-2 and SARS-CoV genomes (Fig. 6). While the RNA secondary structure of the SARS-CoV-2 genome was determined previously by *in vivo* SHAPE analysis (29), we used an *in silico* RNA fold program (30) to predict the RNA secondary structure of the SARS-CoV (Urbani isolate) genome. Our comparative analysis showed the presence of six similar stem-loop structures in the F3 region of SARS-CoV-2 genome and the corresponding region of SARS-CoV genome (Fig. 6). An *in silico* RNA secondary structure analysis of the F3 regions of F3-opt1, F3-opt2, and the F3-opt-chimeras showed the disruption of all six stem-loop structures (SL1 to SL6) in F3-opt1 and F3-opt2, and some of the stem-loop structures in the F3-opt-chimeras (Table 1). As our data suggested the requirement of potentially the entire F3 region for the efficient packaging of SARS2-rep RNAs into virus particles, it is possible that the presence of all six stem-loop structures in the F3 region may be important for viral RNA packaging. Alternatively, a specific core three-dimensional RNA structure, the formation of which is facilitated by the presence of a long flanking sequence in the F3 region, may be required to promote the efficient packaging of SARS-CoV-2 RNA. It is worth noting that the six stem-loop structures in the F3 region of the SARS-CoV-2 genome lack the conserved structural feature of the RNA PS in MHV (16), including the repeated sequence motifs in the stem-loop structure (Fig. 6), suggesting that the packaging-competent structural

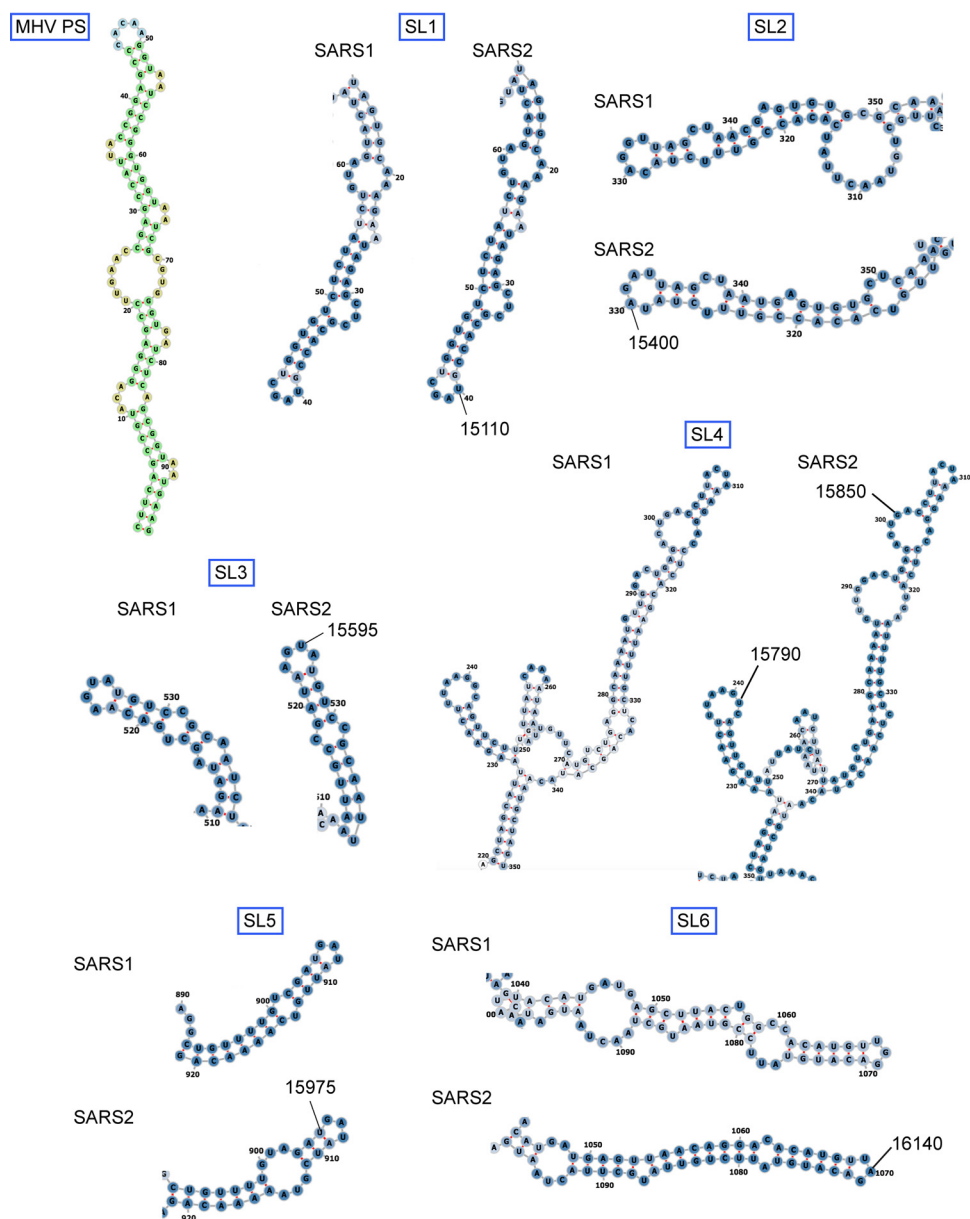


**FIG 6** Predicted stem-loop RNA structures in the F3 region of SARS-CoV-2 (SARS2) and the corresponding region of SARS-CoV (SARS1). SL1 to SL6 represent the six stem-loop structures in SARS-CoV-2 (SARS2) and SARS-CoV (SARS1) RNAs, as determined by an *in vivo* SHAPE analysis (29) and an *in silico* RNA fold program (30), respectively. MHV PS represents the RNA secondary structure of MHV PS (15), which was generated by an RNA secondary structure visualization tool, forna (37).

conformation of viral genomic RNA is not conserved among the subgenera Embecovirus and Sarbecovirus within the Betacoronavirus genus.

## MATERIALS AND METHODS

**Cells and viruses.** Vero-ORF3-E cells (24) and SARS2-delORF3-E virus (24) were obtained from Pei-Yong Shi at the University of Texas Medical Branch (UTMB). The SARS2-delORF3-E virus was generated based on the sequence of the SARS-CoV-2 USA-WA1/2020 strain (MN985325.1) and is a single-cycle replicable mutant, lacking the ORF3 and E genes (24). srSARS-CoV-2 exhibits a single-cycle, replication property in naive cells (24), due to which srSARS-CoV-2 has been approved by the UTMB Biosafety Committee and National Institutes of Health for handling in a BSL2 lab. The SARS2-delORF3-E virus that carried adaptive mutations in nsp1, nsp4, and S genes (24) was amplified in Vero-ORF3-E cells, which coexpress SARS-CoV-2 ORF3 and E proteins in a doxycycline-inducible manner. Vero-ORF3-E cells were maintained in Dulbecco's modified Eagle's medium (DMEM) with 10% fetal bovine serum (FBS), 1% penicillin-streptomycin, and 10  $\mu$ g/mL of puromycin. For the induction of 3a and E protein expression, Vero-ORF3-E cells were incubated in DMEM supplemented with 2% FBS and 100 ng/mL of doxycycline for

**TABLE 1** Disruption of SL structures in F3-opt and F3-opt-chimeras<sup>a</sup>

SL in F3 region	Result of:					
	F3	F3-opt1	F3-opt2	Chimera 1	Chimera 2	Chimera 3
SL1	+	–	–	–	+	+/-
SL2	+	–	–	–	+	+
SL3	+	–	–	–	–	+
SL4	+	–	–	+	–	–
SL5	+	–	–	+	+	–
SL6	+	–	–	+	+	–

<sup>a</sup>SL, step loop; +, SL is maintained; –, SL is not maintained; +/-, SL is partially maintained.

24 h. Vero E6 cells were maintained in DMEM containing 10% FBS and 1% penicillin-streptomycin. For our studies, we used the SARS2-delORF3-E virus that was passaged 4 times in Vero-ORF3-E cells, designated as srSARS-CoV-2. The recombinant infectious clone of SARS-CoV-2 used in this study was generated using the SARS-CoV-2 reverse genetics system, according to established protocols, as described previously (31). The titers of SARS-CoV-2 and srSARS-CoV-2 were determined by standard plaque assay in Vero E6 and Vero-ORF3-E cells, respectively. The SARS-CoV Urbani strain (AY278741.1) was grown in Vero E6 cells.

**Purification of virus released from srSARS-CoV-2-infected cells.** Vero-ORF3-E cells were treated with doxycycline for 24 h and infected with srSARS-CoV-2. Intracellular RNA and culture supernatants were harvested at 30 h p.i. Sucrose solutions were prepared in NTE buffer (0.1 M NaCl, 10 mM Tris-HCl [pH 7.5], and 1 mM EDTA). Culture supernatant was clarified by centrifugation at 800 × g for 15 min at 4°C and subjected to sucrose gradient ultracentrifugation, using a 20% to 60% continuous sucrose gradient, at 4°C for 18 h at 26,000 rpm using a SW28 rotor (Beckman). Twelve fractions (1.6 mL each) were collected from the bottom of the tube. The collected fractions were diluted with NTE buffer and pelleted by ultracentrifugation through a 20% sucrose cushion at 4°C for 2 h at 38,000 rpm using a SW41 rotor (Beckman). For protein analysis, the pellets were suspended in sodium dodecyl sulfate-polyacrylamide gel electrophoresis (SDS-PAGE) sample buffer and incubated at 37°C for 30 min. For RNA analysis, the pellets were suspended in TRIzol reagent (Ambion) and RNAs were extracted according to the manufacturer's protocol.

**Serial passage of SARS-CoV in Vero E6 cells.** Serial undiluted passage of SARS-CoV was performed in a blind manner in Vero E6 cells until passage 23. Culture fluid was collected at 24 h to 48 h postinfection (p.i.). The virus supernatant from different passages was used to infect naive Vero E6 cells, and intracellular RNAs were extracted at 18 h p.i. Total RNA was extracted from the SARS-CoV-infected cells and subjected to cDNA synthesis using random primers. The DNA fragment was amplified by PCR using a forward primer (5'-CGCAGTATAACAATAATAAATTTACTGTCGTTGAC -3'), which binds to the 5' untranslated region (UTR) of SARS-CoV genomic RNA, immediately downstream of the leader sequence, and a reverse primer (5'-GTCATTCTCCTAAGAAG -3'), which binds to the 3' UTR of SARS-CoV genomic RNA. The sequence of the DNA fragment was determined by Sanger sequencing, and the sequence data were deposited to GenBank (accession number OR113691).

**Plasmid construction and *in vitro* RNA synthesis.** All the plasmids encoding SARS2-rep RNAs were designed based on the sequence of the SARS-CoV-2 USA-WA1/2020 strain (MN985325.1) (32, 33). For the construction of the plasmid encoding SARS2-rep-rLuc RNA (Fig. 3A), we generated a DNA fragment, composed of the 5'-end region of the SARS-CoV-2 genome, which included a partial sequence of the nsp1 ORF fused to the rLuc gene, the 3'-end region of SARS-CoV-2 genome, and a 29-nt-long poly(A) tail sequence, along with an Esp3I site for plasmid linearization, by recombinant PCR. The DNA fragment was inserted into the T7-promoter-containing pT7 plasmid (34). The plasmid encoding the SARS2-rep RNA carrying F1 fragment (Fig. 3A) was also generated by recombinant PCR as described above, except that the F1 sequence was used in place of the rLuc gene. A BstBI restriction enzyme site was inserted between the F1 sequence and the 3'-end sequence in the plasmid encoding the SARS2-rep RNA carrying F1 region, to facilitate the cloning of plasmids encoding SARS2-rep RNAs, carrying the F2 to F7 fragments (Fig. 3A). Plasmids encoding SARS2-rep RNAs, carrying the F2 to F7 regions, were generated by replacing the F1 fragment with other fragments using NdeI and BstBI restriction sites (Fig. 3A). For the fragments carrying the internal BstBI site, blunt end cloning was performed to insert the fragments. The plasmids were linearized using Esp3I and were purified by phenol-chloroform extraction. For the fragments carrying an internal Esp3I site, a BciVI site was inserted after the poly(A) sequence and used for linearization. Next, 5'-capped mRNAs were synthesized using the mMessage mMachine T7 transcription kit (ThermoFisher Scientific).

**Assay to determine the packaging efficiency of SARS-CoV-2 minigenome RNAs.** Vero E6 cells were infected with SARS-CoV-2 at a multiplicity of infection (MOI) of 1. After 1 h of incubation, cells were transfected with *in vitro*-synthesized RNA using the TransIT mRNA reagent (Mirus). Infected cell lysates and culture supernatants (P0 virus) were harvested at 19 h p.i. Vero E6 cells were inoculated with P0 virus supernatant, and total RNA was extracted from the P0-infected cells at 20 h p.i. using TRIzol reagent (Ambion) and analyzed by Northern blotting. The intensity of bands in the chemiluminescent Northern blots was quantified by densitometry using Fiji software (version 2.3.0).

For the experiment using Vero-ORF3-E cells, doxycycline-treated Vero-ORF3-E cells were infected with srSARS-CoV-2 at an MOI of 0.1, followed by transfection with *in vitro*-synthesized RNA using TransIT mRNA reagent (Mirus) after 1 h of incubation with the virus. Infected cell lysates and culture supernatants (P0 virus) were harvested at 24 h to 30 h p.i. Doxycycline-treated Vero-ORF3-E cells were inoculated with the P0 virus sample, and intracellular RNAs were extracted 24 h to 30 h p.i. using TRIzol reagent (Ambion).

For the purification of virus particles, carrying the SARS-CoV-2 minigenome RNAs, doxycycline-treated Vero-ORF3-E cells were infected with srSARS-CoV-2 at an MOI of 0.5. After 1 h of virus inoculation, cells were transfected with *in vitro*-synthesized RNA using the TransIT mRNA reagent (Mirus). After 1 h posttransfection, the cells were washed twice with PBS and incubated in culture media. Culture supernatant was harvested at 27 h p.i., clarified by low-speed centrifugation at  $800 \times g$  for 15 min at 4°C, and subjected to sucrose gradient ultracentrifugation, using a discontinuous sucrose gradient consisting of 60, 50, 30, and 20% sucrose (wt/vol) in NTE buffer, at 4°C for 18 h at 26,000 rpm using a SW28 rotor (Beckman). The particles at the interface between 30 and 50% were collected and pelleted by ultracentrifugation through a 20% sucrose cushion at 4°C for 2 h at 38,000 rpm using a SW41 rotor (Beckman). The pellets were suspended in SDS sample buffer for protein analysis and TRIzol reagent for RNA analysis.

**Northern blot.** For the detection of SARS-CoV RNAs, we used two digoxigenin (DIG)-labeled DNA probes, namely, one corresponding to the nucleotide positions 81 to 420 from the 5' end of the SARS-CoV genome to detect the SARS-CoV genomic RNA (5'-end probe) and the other corresponding to nucleotide positions 29084 to 29608 of the SARS-CoV genome to detect all the SARS-CoV mRNAs (3'-end probe). These probes were generated using DIG-high prime DNA labeling and detection starter kit II (Roche). For the detection of SARS-CoV-2 RNAs, a DIG-labeled RNA probe (5'-end probe) corresponding to nucleotide positions 84 to 600 from the 5' end of the SARS-CoV-2 genome was generated using a DIG RNA labeling kit (Roche). A DIG-labeled DNA probe (31) (3'-end probe), corresponding to nucleotide positions 28999 to 29573 of the SARS-CoV-2 genome, was generated using DIG-high prime DNA labeling and detection starter kit II (Roche). The same amount of total RNA was separated on a 1.2% denaturing agarose-formaldehyde gel and transferred onto a nylon membrane (Roche). Detection was performed using a DIG luminescent detection kit (Roche Applied Science).

**Western blot.** Western blot was performed as described previously (35). Rabbit anti-SARS-CoV N polyclonal antibody (32) and rabbit anti-SARS-CoV M polyclonal antibody (36) (a gift from Carolyn Machamer at Johns Hopkins University) were used. A goat anti-rabbit horseradish peroxidase (HRP)-linked antibody was used as a secondary antibody (Cell Signaling Technology). A conformation-specific mouse anti-rabbit antibody (Cell Signaling Technology) was used as a secondary antibody for the Western blot analysis of immunoprecipitated samples.

**In silico RNA secondary structure analysis.** A web-based *in silico* RNA fold program (30) (<http://rna.tbi.univie.ac.at/cgi-bin/RNAWebSuite/RNAfold.cgi>) was used for the RNA secondary structure analysis. *forna*, an RNA secondary structure visualization tool (37) (<http://rna.tbi.univie.ac.at/forna/>), was used to graphically display the secondary structure of MHV PS.

## ACKNOWLEDGMENTS

We thank Pei-Yong Shi at UTMB for providing us with the Vero-ORF3-E cells and SARS2-delORF3-E virus and Carolyn Machamer at Johns Hopkins University for providing the anti-M antibody.

This study was supported by Public Health Service grant AI146081 from the National Institutes of Health to SM and a COVID-19 grant and a Pilot Grant from the Institute for Human Infections and Immunity at UTMB to K.T. and S.M., respectively.

We declare no competing interests.

## REFERENCES

- Lamers MM, Haagmans BL. 2022. SARS-CoV-2 pathogenesis. *Nat Rev Microbiol* 20:270–284. <https://doi.org/10.1038/s41579-022-00713-0>.
- Zhang Y, Geng X, Tan Y, Li Q, Xu C, Xu J, Hao L, Zeng Z, Luo X, Liu F, Wang H. 2020. New understanding of the damage of SARS-CoV-2 infection outside the respiratory system. *Biomed Pharmacother* 127:110195. <https://doi.org/10.1016/j.biopha.2020.110195>.
- Healey Q, Sheikh A, Daines L, Vasileiou E. 2022. Symptoms and signs of long COVID: a rapid review and meta-analysis. *J Glob Health* 12:e05014. <https://doi.org/10.7189/jogh.12.05014>.
- Uraki R, Ito M, Furusawa Y, Yamayoshi S, Iwatsuki-Horimoto K, Adachi E, Saito M, Koga M, Tsutsumi T, Yamamoto S, Otani A, Kiso M, Sakai-Tagawa Y, Ueki H, Yotsuyanagi H, Imai M, Kawaoka Y. 2023. Humoral immune evasion of the omicron subvariants BQ.1.1 and XBB. *Lancet Infect Dis* 23:30–32. [https://doi.org/10.1016/S1473-3099\(22\)00816-7](https://doi.org/10.1016/S1473-3099(22)00816-7).
- Anonymous. 2022. Overview of COVID-19 vaccines. Centers for Disease Control and Prevention, Atlanta, GA.
- Ashour NA, Abo Elmaaty A, Sarhan AA, Elkaeed EB, Moussa AM, Erfan IA, Al-Kamalawy AA. 2022. A systematic review of the global intervention for SARS-CoV-2 combating: from drugs repurposing to molnupiravir approval. *Drug Des Devel Ther* 16:685–715. <https://doi.org/10.2147/DDDT.S354841>.
- V'kovski P, Kratzel A, Steiner S, Stalder H, Thiel V. 2021. Coronavirus biology and replication: implications for SARS-CoV-2. *Nat Rev Microbiol* 19:155–170. <https://doi.org/10.1038/s41579-020-00468-6>.
- Jackson CB, Farzan M, Chen B, Choe H. 2022. Mechanisms of SARS-CoV-2 entry into cells. *Nat Rev Mol Cell Biol* 23:3–20. <https://doi.org/10.1038/s41580-021-00418-x>.
- Ruch TR, Machamer CE. 2012. The coronavirus E protein: assembly and beyond. *Viruses* 4:363–382. <https://doi.org/10.3390/v4030363>.
- Kuo L, Hurst-Hess KR, Koetzner CA, Masters PS. 2016. Analyses of coronavirus assembly interactions with interspecies membrane and nucleocapsid protein chimeras. *J Virol* 90:4357–4368. <https://doi.org/10.1128/JVI.03212-15>.
- Zhang Z, Nomura N, Muramoto Y, Ekimoto T, Uemura T, Liu K, Yui M, Kono N, Aoki J, Ikeguchi M, Noda T, Iwata S, Ohto U, Shimizu T. 2022. Structure of SARS-CoV-2 membrane protein essential for virus assembly. *Nat Commun* 13:4399. <https://doi.org/10.1038/s41467-022-32019-3>.
- Mariano G, Farthing RJ, Lale-Farjat SLM, Bergeron JRC. 2020. Structural characterization of SARS-CoV-2: where we are, and where we need to be. *Front Mol Biosci* 7:605236. <https://doi.org/10.3389/fmolb.2020.605236>.
- Makino S, Yokomori K, Lai MM. 1990. Analysis of efficiently packaged defective interfering RNAs of murine coronavirus: localization of a possible RNA-packaging signal. *J Virol* 64:6045–6053. <https://doi.org/10.1128/JVI.64.12.6045-6053.1990>.
- Escors D, Izeta A, Capiscol C, Enjuanes L. 2003. Transmissible gastroenteritis coronavirus packaging signal is located at the 5' end of the virus genome. *J Virol* 77:7890–7902. <https://doi.org/10.1128/jvi.77.14.7890-7902.2003>.

15. Kuo L, Masters PS. 2013. Functional analysis of the murine coronavirus genomic RNA packaging signal. *J Virol* 87:5182–5192. <https://doi.org/10.1128/JVI.00100-13>.
16. Masters PS. 2019. Coronavirus genomic RNA packaging. *Virology* 537:198–207. <https://doi.org/10.1016/j.virol.2019.08.031>.
17. Narayanan K, Makino S. 2001. Cooperation of an RNA packaging signal and a viral envelope protein in coronavirus RNA packaging. *J Virol* 75:9059–9067. <https://doi.org/10.1128/JVI.75.19.9059-9067.2001>.
18. Molenkamp R, Spaan WJ. 1997. Identification of a specific interaction between the coronavirus mouse hepatitis virus A59 nucleocapsid protein and packaging signal. *Virology* 239:78–86. <https://doi.org/10.1006/viro.1997.8867>.
19. Kuo L, Koetzner CA, Masters PS. 2016. A key role for the carboxy-terminal tail of the murine coronavirus nucleocapsid protein in coordination of genome packaging. *Virology* 494:100–107. <https://doi.org/10.1016/j.virol.2016.04.009>.
20. Hsieh PK, Chang SC, Huang CC, Lee TT, Hsiao CW, Kou YH, Chen IY, Chang CK, Huang TH, Chang MF. 2005. Assembly of severe acute respiratory syndrome coronavirus RNA packaging signal into virus-like particles is nucleocapsid dependent. *J Virol* 79:13848–13855. <https://doi.org/10.1128/JVI.79.22.13848-13855.2005>.
21. Syed AM, Taha TY, Tabata T, Chen IP, Ciling A, Khalid MM, Sreekumar B, Chen PY, Hayashi JM, Soczek KM, Ott M, Doudna JA. 2021. Rapid assessment of SARS-CoV-2-evolved variants using virus-like particles. *Science* 374:1626–1632. <https://doi.org/10.1126/science.abc16184>.
22. Hsin WC, Chang CH, Chang CY, Peng WH, Chien CL, Chang MF, Chang SC. 2018. Nucleocapsid protein-dependent assembly of the RNA packaging signal of Middle East respiratory syndrome coronavirus. *J Biomed Sci* 25:47. <https://doi.org/10.1186/s12929-018-0449-x>.
23. Chen SC, Olsthoorn RCL. 2010. Group-specific structural features of the 5'-proximal sequences of coronavirus genomic RNAs. *Virology* 401:29–41. <https://doi.org/10.1016/j.virol.2010.02.007>.
24. Zhang X, Liu Y, Liu J, Bailey AL, Plante KS, Plante JA, Zou J, Xia H, Bopp NE, Aguilar PV, Ren P, Menachery VD, Diamond MS, Weaver SC, Xie X, Shi PY. 2021. A trans-complementation system for SARS-CoV-2 recapitulates authentic viral replication without virulence. *Cell* 184:2229–2238.e13. <https://doi.org/10.1016/j.cell.2021.02.044>.
25. van der Most RG, Bredenbeek PJ, Spaan WJ. 1991. A domain at the 3' end of the polymerase gene is essential for encapsidation of coronavirus defective interfering RNAs. *J Virol* 65:3219–3226. <https://doi.org/10.1128/JVI.65.6.3219-3226.1991>.
26. Méndez A, Smerdou C, Izeta A, Gebauer F, Enjuanes L. 1996. Molecular characterization of transmissible gastroenteritis coronavirus defective interfering genomes: packaging and heterogeneity. *Virology* 217:495–507. <https://doi.org/10.1006/viro.1996.0144>.
27. Penzes Z, Tibbles K, Shaw K, Britton P, Brown TD, Cavanagh D. 1994. Characterization of a replicating and packaged defective RNA of avian coronavirus infectious bronchitis virus. *Virology* 203:286–293. <https://doi.org/10.1006/viro.1994.1486>.
28. Girgis S, Xu Z, Oikonomopoulos S, Fedorova AD, Tchesnokov EP, Gordon CJ, Schmeing TM, Götte M, Sonenberg N, Baranov PV, Ragoussis J, Hobman TC, Pelletier J. 2022. Evolution of naturally arising SARS-CoV-2 defective interfering particles. *Commun Biol* 5:1140. <https://doi.org/10.1038/s42003-022-04058-5>.
29. Sun L, Li P, Ju X, Rao J, Huang W, Ren L, Zhang S, Xiong T, Xu K, Zhou X, Gong M, Miska E, Ding Q, Wang J, Zhang QC. 2021. In vivo structural characterization of the SARS-CoV-2 RNA genome identifies host proteins vulnerable to repurposed drugs. *Cell* 184:1865–1883.e20. <https://doi.org/10.1016/j.cell.2021.02.008>.
30. Gruber AR, Lorenz R, Bernhart SH, Neuböck R, Hofacker IL. 2008. The Vienna RNA website. *Nucleic Acids Res* 36:W70–W74. <https://doi.org/10.1093/nar/gkn188>.
31. Xie X, Muruato A, Lokugamage KG, Narayanan K, Zhang X, Zou J, Liu J, Schindewolf C, Bopp NE, Aguilar PV, Plante KS, Weaver SC, Makino S, LeDuc JW, Menachery VD, Shi PY. 2020. An infectious cDNA clone of SARS-CoV-2. *Cell Host Microbe* 27:841–848.e3. <https://doi.org/10.1016/j.chom.2020.04.004>.
32. Harcourt J, Tamin A, Lu X, Kamili S, Sakthivel SK, Murray J, Queen K, Tao Y, Paden CR, Zhang J, Li Y, Uehara A, Wang H, Goldsmith C, Bullock HA, Wang L, Whitaker B, Lynch B, Gautam R, Schindewolf C, Lokugamage KG, Scharton D, Plante JA, Mirchandani D, Widen SG, Narayanan K, Makino S, Ksiazek TG, Plante KS, Weaver SC, Lindstrom S, Tong S, Menachery VD, Thornburg NJ. 2020. Severe acute respiratory syndrome coronavirus 2 from patient with coronavirus disease, United States. *Emerg Infect Dis* 26:1266–1273. <https://doi.org/10.3201/eid2606.200516>.
33. Holshue ML, DeBolt C, Lindquist S, Lofy KH, Wiesman J, Bruce H, Spitters C, Ericson K, Wilkerson S, Tural A, Diaz G, Cohn A, Fox L, Patel A, Gerber SI, Kim L, Tong S, Lu X, Lindstrom S, Pallansch MA, Weldon WC, Biggs HM, Uyeki TM, Pillai SK, Washington State 2019-nCoV Case Investigation Team. 2020. First case of 2019 novel coronavirus in the United States. *N Engl J Med* 382:929–936. <https://doi.org/10.1056/NEJMoa2001191>.
34. Ikegami T, Won S, Peters CJ, Makino S. 2006. Rescue of infectious rift valley fever virus entirely from cDNA, analysis of virus lacking the NSs gene, and expression of a foreign gene. *J Virol* 80:2933–2940. <https://doi.org/10.1128/JVI.80.6.2933-2940.2006>.
35. Terasaki K, Ramirez SI, Makino S. 2016. Mechanistic insight into the host transcription inhibition function of Rift valley fever virus NSs and its importance in virulence. *PLoS Negl Trop Dis* 10:e0005047. <https://doi.org/10.1371/journal.pntd.0005047>.
36. McBride CE, Li J, Machamer CE. 2007. The cytoplasmic tail of the severe acute respiratory syndrome coronavirus spike protein contains a novel endoplasmic reticulum retrieval signal that binds COPI and promotes interaction with membrane protein. *J Virol* 81:2418–2428. <https://doi.org/10.1128/JVI.02146-06>.
37. Kerpedjiev P, Hammer S, Hofacker IL. 2015. Forna (force-directed RNA): simple and effective online RNA secondary structure diagrams. *Bioinformatics* 31:3377–3379. <https://doi.org/10.1093/bioinformatics/btv372>.